1 Pan-Arctic soil element availability estimations

2 Peter Stimmler[1], Mathias Goeckede[2], Bo Elberling[3], Susan Natali[4], Peter Kuhry[5], Nia Perron[6],
3 Fabrice Lacroix[2], Gustaf Hugelius[5,7], Oliver Sonnentag[6], Jens Strauss[8], Christina Minions[4],
4 Michael Sommer[1], and Jörg Schaller[1*]

6 [1] Leibniz Centre for Agricultural Landscape Research (ZALF), Müncheberg, Germany
7 [2] Max Planck Institute for Biogeochemistry, Jena, Germany
8 [3] Center for Permafrost, Department of Geosciences and Natural Resource Management, University of Copenhagen,
9 Copenhagen, Denmark
10 [4] Woodwell Climate Research Center, Falmouth, USA
11 [5] University Stockholm, Stockholm, Sweden
12 [6] Département de Géographie, Université de Montréal, 1375 Avenue Thérèse-Lavoie-Roux, Montréal, QC H2V 0B3,
13 Canada
14 [7] Bolin Centre for Climate Research, Stockholm University, Stockholm, Sweden
15 [8] Alfred Wegener Institute Helmholtz Centre for Polar and Marine Research, Permafrost Research Section, Potsdam,
16 Germany

18 *Correspondence to: email: Joerg.Schaller@zalf.de

20 **Abstract.** Arctic soils store large amounts of organic carbon and other elements such as amorphous silica, silicon,

21 calcium, iron, aluminium, and phosphorous. Global warming is projected to be most pronounced in the Arctic leading

22 to thawing permafrost, which in turn is changing the soil element availability. To project how biogeochemical cycling

23 in Arctic ecosystems will be affected by climate change, there is a need for data on element availability. Here, we

24 analysed amorphous silica (ASi), silicon (Si), calcium (Ca), iron (Fe), phosphorus (P), and aluminium (Al) availability

25 from 574 soil samples from the circumpolar Arctic region. We show large differences in ASi, Si, Ca, Fe, P, and Al

26 availability among different lithologies and Arctic regions. We summarized these data in pan-Arctic maps of ASi, Si,

27 Ca, Fe, P, and Al concentrations focussing on the top 100 cm of Arctic soil. Furthermore, we provide values for

28 element availability for the organic and the mineral layer of the seasonally thawing active layer as well as for the

29 uppermost permafrost layer. Our spatially explicit data on differences in the availability of elements between the

30 different lithological classes and regions now and in the future will improve Arctic Earth system models for estimating

31 current and future carbon and nutrient feedbacks under climate change.

1 Introduction

Temperatures in northern high latitude region have risen more than twice as fast as the global average within the last decades (IPCC, 2021). This warming leads to thawing of perennially frozen ground known as permafrost (Brown and Romanovsky, 2008; Romanovsky et al., 2010). Frozen conditions prevent organic matter (OM) from microbial degradation and also limits fluvial export of soil-bound nutrients to the sea by runoff (Mann et al., 2022). Thawing of frozen ground (defined as permafrost soils in the following) may in turn accelerate global warming by potentially releasing potent greenhouse gases such as carbon dioxide (CO_2) and methane (CH_4) through soil organic carbon mineralization (Schuur et al., 2015). The frozen ground of the Arctic-boreal regions (hereafter called 'Arctic', but also including subarctic regions) are the largest pool of soil organic carbon worldwide. Approximately, 1014 - 1035 ± max. 194 Pg of organic carbon is stored within the upper 3 m of permafrost region soils (Hugelius et al., 2014; Mishra et al., 2021). To full depth, ca. 1460 - 1600 Pg carbon is stored in the permafrost region (Strauss et al., 2021a), and approximately one third of this is in ice rich Yedoma deposits, exceeding 3m depth (Fuchs et al., 2018; Strauss et al., 2017). The Yedoma deposits formed in unglaciated areas of the northern hemisphere during the glacial period, when melt water from glacial areas and eolian processes transported fine sediment to the unglaciated lowlands (Schuur et al., 2013; Strauss et al., 2021b; Strauss et al., 2013). Yedoma deposits are characterized by high carbon and water content. The water is mostly bound in massive ice in ice wedges as well as segregated ice and pore ice in sediment columns (Schirrmeister et al., 2011). Thus, Yedoma soils are highly vulnerable to thawing as the loss of the high ice volume leads to surface subsidence and thermokarst processes, which can accelerate thaw and remobilize deep elemental stocks.

The temperature and near-surface water content in the Arctic soils have changed rapidly in the last decades and further changes are expected in future (Box et al., 2019). An important effect of Arctic warming is a deepening of the seasonally-thawed active layer and related thermokarst processes, which may lead to a mobilization of nutrients from permafrost soil layers (Abbott et al., 2015). Additionally, increased temperatures in the Arctic regions may accelerate weathering, potentially enhancing nutrient availability in terrestrial Arctic ecosystems and export to freshwater systems, and finally to the nearshore zone and sea (Holmes et al., 2013).

As the Arctic features a mineral composition of the sediments that is different from many other global soils (Monhonval et al., 2021a), the availability (for microbes and plants) of elements in Arctic soils may differ as well. Yedoma deposits, for example, are important pools of OM in the Arctic. Because Yedoma deposits include materials transported from nearby mountains, the mineral compositions of the Yedoma soils depend on the original geology of the mountains (Schirrmeister et al., 2011). Sediments of marine origin are often rich in calcium (Ca), phosphorus (P) and silicon (Si), while magmatic rocks such as granite or basalt contain large amounts of Si, iron (Fe), aluminum (Al), and P. The availability of these elements in soils is the complex product of soil genesis and nutrient release, which depend on physical and chemical conditions including temperature, water content and pH. In this context, Si, Ca, Fe, Al or P are bound in or on mineral phases and are released via enzymatic activity or weathering. Ongoing Arctic climate warming now threatens to disturb the pools that have equilibrated to conditions characteristic for the past millennia.

69   The availability of elements such as P, Fe, Ca, and Si in soils are known controls for soil OM respiration (Brady and
70   Weil, 2008; Schaller et al., 2019). A release of inorganic nutrients such as P or Si can lead to increased greenhouse
71   gas production and potentially to further export of this elements to the fresh and seawaters. In marine systems, P, Fe,
72   Ca, and Si are well-known to control carbon (C) fixation in terms of algae biomass productivity (Tremblay et al.,
73   2015). In terrestrial systems, P availability is positively related to silicic acid ($Si(OH)_4$) (Schaller et al., 2019) or its
74   polymers, which mobilize from, e.g., amorphous silica (ASi) (Schaller et al., 2021). The mobilization of P by Si was
75   shown to occur due to competition for binding at Fe-minerals (Schaller et al., 2019), which tend to strongly bind P
76   under condition of low Si availability (Gérard, 2016). Contrary to Si, Ca bind P by calcium phosphate co-precipitation
77   with calcium carbonate, at least under high soil pH conditions (Otsuki and Wetzel, 1972). Like P, OM is also binding
78   to Ca, Fe and Al-phases (Kaiser and Zech, 1997; Wiseman and Püttmann, 2006) but being mobilized from those
79   phases by Si (Hömberg et al., 2020). If the Fe availability in soils is low, the binding of P may be related to Al-minerals
80   (Eriksson et al., 2015).

81   Despite the important role of soil elements in driving soil and ecosystem processes and the potential for rapid changes
82   in the Arctic due to climate change, the spatial distribution of elemental stocks (beyond C, N) is not well understood.
83   An ecologically based classification of soil Ca concentrations was proposed by Walker et al. (2001), differentiating
84   between a Ca rich non-acidic tundra and a Ca poor acidic tundra based on differences in vegetation types for the
85   Alaskan Arctic region. This classification system was further used to estimate pan-Arctic soil OM stocks (Hugelius et
86   al., 2014), which proved to be a useful approach as vegetation is tightly connected to OM stocks (Quideau et al., 2001).
87   Based on the work of Hugelius et al. (2014), Alfredsson et al. (2016) related vegetation cover to amorphous Si (ASi)
88   concentration to scale up Arctic ASi stocks. However, in contrast to OM stocks being clearly related to vegetation
89   (Hugelius et al., 2014), the effect of vegetation on mineral availability in soils is debatable. Therefore, the extrapolation
90   of circum-polar Arctic maps of element availability for P, Fe, Ca, Al, and Si based on vegetation distribution alone
91   may be associated with high uncertainties. A much stronger driver of element availability could be parent material
92   and lithology (Alloway, 2013).

93   In this study, we aim to map pan-Arctic soil element bio-availability (for microbes and plants) by applying a lithology-
94   based extrapolation of plot level sampling data on nutrient availability. We provide maps for ASi, Si, Ca, Fe, P and
95   Al as these elements have direct effects on OM binding and greenhouse gas (GHG) emission from the circumpolar
96   Arctic. In addition, these elements are limiting nutrients for CO_2 binding in terms of primary production in Arctic
97   marine systems or interfere with those. Better understanding of element availability is crucial to reduce uncertainties
98   for reliable modelling of future scenarios on how Arctic system may respond to global warming.

2 Material and Methods

2.1 General approach

Based on the Geological Map of the Arctic (Harrison et al., 2011), we estimate the bio-availability and potential mobility of ASi, Si, Ca, Fe, Al and P in Arctic soils. We analyzed soil samples from organic, mineral and permafrost layers from pan-Arctic sampling campaigns. We used the biological available element concentrations of certain lithologies to compile pan-Arctic maps covering 7.6×10^6 km² for ASi, mineral Si, Ca, Fe, Al and P.

2.2 Sampling and storage

In total, we analyzed 574 Arctic soil samples from 25 locations (Fig. 1). To ensure a pan-Arctic coverage we analyzed samples from Siberia (222 samples from six locations), North America (115 samples from six locations), Greenland (111 samples from nine locations), Northern Europe (13 samples from one location) and Svalbard (103 samples from three locations) (Fig. 1 and S1, Table S1). We analyzed samples from the thawed near-surface organic layer (252 soil samples, mainly 0-20 cm in depth), mineral layer (208 soil samples, mainly 20-50 cm depth)) and permafrost layer (104 soil samples, mainly 50-100 cm depth). We split the annually thawed active layer in the upper organic layer and the mineral layer below by C content, except for soils where the organic layer corresponds to the active layer. The organic layer contained mainly organic matter (OM) in different mineralization states. The mineral soil layer has variable OM content depending on which soil processes have affected this layer and reaches to the perennially frozen permafrost layer. We took samples using an auger or a spade and stored them frozen until analysis or as described before (Faucherre et al., 2018; Kuhry et al., 2020). Samples consisted of 5-50 g frozen soil. Before analysis, the samples were oven dried and ground.

2.3 Extraction and analysis

Available concentrations of Si, Ca, Fe, Al and P were quantified using the Mehlich III method (Sims, 1989). Briefly, we extracted 0.5 to 5 g of freeze-dried soil using 10 ml g-1 Mehlich III solution (0.015 M NH4F, 0.001 M EDTA, 0.25 M NH4NO3, 0.00325 M HNO3, 0.2 M HAc). The samples were shaken for 5 min at 200 min-1 and centrifuged for 5 min at 10.000 x g. Afterwards, the supernatant was filtered using a 0.2 μm cellulose acetate filter. The analysis was done by inductive coupled plasma with optical emission spectroscopy (ICP-OES) (Vista-PRO radial, Varian Medical Systems, Palo Alto, California). For extraction of available amorphous silica (ASi) an alkaline extraction was used (DeMaster 1981), extracting ASi from 30 mg of freeze-dried soil using 40 ml 0.1 M Na2CO3 solution at 85°C for 5 h. After 1 h, 3 h and 5 h the suspension was mixed, and 10 ml of the supernatant was subsampled, filtered by a 0.2 μm cellulose acetate filter and analyzed by ICP-OES. The ASi concentration was calculated using a linear regression of ASi concentration in solution over time and the intersection with the Y-axis was used as concentration of available concentration according to DeMaster (1981). To determine the dry weight (DW) of the samples 0.5-2 g of frozen material was freeze dried until weight constancy.

2.4 Statistics

2.4.1 Statistics and graphics

Data were analyzed using the R Studio (R_Core_Team, 2021). We extracted the original data (lithology, location, geometry) given for GIS polygons (shape files from the different regions, Greenland, Can_USA, Ice, N_Europa_Russia) of the Geological Map of the Arctic containing locations. We extracted 14 lithological classes in total. We matched the soil sampling locations for which we obtained data for element availability by extraction (see above) with the GIS polygons (geology) by ARCView_GIS_3.2 extensions "Spatial Analyst" command "analysis: tabulate Areas". The sum of areas with the same map label was extracted by map label "shape area". We considered only terrestrial areas. For every location, we calculated the element concentrations for the different samples from organic, mineral and permafrost layer. We calculated quantiles, mean and standard error using "summarise" from the "dplyr" R package. We clustered element concentration data for all locations by lithological class and calculated mean and standard error for organic, mineral and permafrost layer. The number of samples for each lithological class is given in Fig. 1.

2.4.2 Element concentration maps

We used the "Geological Map of the Arctic (1:5 000 000 scale, in the Arctic polar region, north of latitude 60°N") as the basis for our maps. We calculated the weighted numeric mean concentration for each element in the first 100 cm from the soil surface using formula (1). The mean mass fraction (wm) of an element (X) is the sum of the products of the mass fractions in organic (OL), mineral (ML) and permafrost (PL) layer and the thickness (d) of each layer in cm divided by 100 cm. We colored the represented area based on the element concentration.

$$w_m(X)\left[\frac{mg}{g}\right] = \frac{\left(w_{OL}(X)\left[\frac{mg}{g}\right]*d_{OL}\,[m]+w_{ML}(X)\left[\frac{mg}{g}\right]*d_{ML}\,[m]+w_{PL}(X)\left[\frac{mg}{g}\right]*d_{PL}\,[m]\right)}{100\,[cm]} \qquad \text{(eq. 1)}$$

3 Results

3.1 Geographical and lithological representation

Our sampling locations represent 13 out of 17 original geographic domains (missing: North Asia and North America, ice, none assigned), defined by the base map (76.5 %) (Table 1, Fig. S1 and Table S2) of the Arctic. The single areas and shares for the maps of Canada/Alaska, Greenland and North Europe/Russia are given in Table S3. Our data represent 17 eras of the Geological Map of the Arctic. The age ranged between 2.6 and 2,500 mya. The number of samples per age code are shown in Fig S2. Our data represent 14 lithological classes of the "Geological Map of the Arctic" (Table S4). These 14 lithological classes represent 7.63×10^{12} m² out of 1.57×10^{13} m² (48.49 % of the area represented by the Geological Map of the Arctic, including ice sheets). Sediments cover 1.03×10^{13} m² of the Arctic. Our data represent sedimentary classes that cover 6.77×10^{12} m² (65.9 % of the Arctic sediment cover) (Fig. S3). In total 3.68×10^{11} m² of 7.37×10^{11} m² (49.9 %) of Yedoma deposits were represented (Fig. S4). The 14 lithological classes can be observed in the igneous type (extrusive: mafic. class 1, n=26), type unclassified (Metamorphic undivided: class 2, n=21) and the sedimentary type (Carbonate: class 3, n=24; class 4, n=58; class 5, n=64; Clastic: shallow marine: class 6, n=13; Clastic: deltaic and nearshore: class 7, n=68; Sedimentary: undivided: class 8, n=38; class 9, n=39; Clastic: shallow marine: class 10, n=91; class 11, n=60; Sedimentary and/or volcanic: undivided: class 12, n=21; and Slope and deep water: class 13, n=43; class 14, n=8).

171 **Table 1**: First column lists original parameters given by the Geological Map of the Arctic (Harrison et al., 2011) and
172 Yedoma deposits (Strauss et al., 2021b). The column "Represented" gives absolute numbers for chronological or
173 lithological classes and of the area extrapolated by this study. For the area, relative share in comparison to total area
174 given by original studies is given, too.

Parameter	Represented	Explanation	Example
Geographic domain	13 (76.5%)	"Phanerozoic regions are based on major physiographic features of the Arctic" (Harrison et al., 2011)	Interior western Alaska
Era	17 (2.6 – 2,500 mya)	"Standardization of map-unit attributes has been facilitated by the International Stratigraphic Chart (August 2009 version) published by the International Commission on Stratigraphy (ICS)" (Harrison et al., 2011)	Neogene (23.0 - 2.6 Ma)
Represented area	7.63×10^{12} m² (43.03%)	Area of the Geological Map of the Arctic (Harrison et al., 2011) containing own data to element concentrations (Fig. 3-8).	
Lithological class	14	Specification and examples of rock type	Lithological class 2: Gneiss, migmatite; reworked amphibolite and granulite facies rocks
Sediments	6.77×10^{12} m² (65.9%)	Areas with lithological classes of the sedimentary type	Lithological class 7: Sandstone, siltstone, shale, coal; plant fossils; metamorphic grade not identified
Yedoma deposition	3.68×10^{11} m² (49.9%)	Areas that contain Yedoma deposits defined by Strauss et al. (2021b)	

175

176
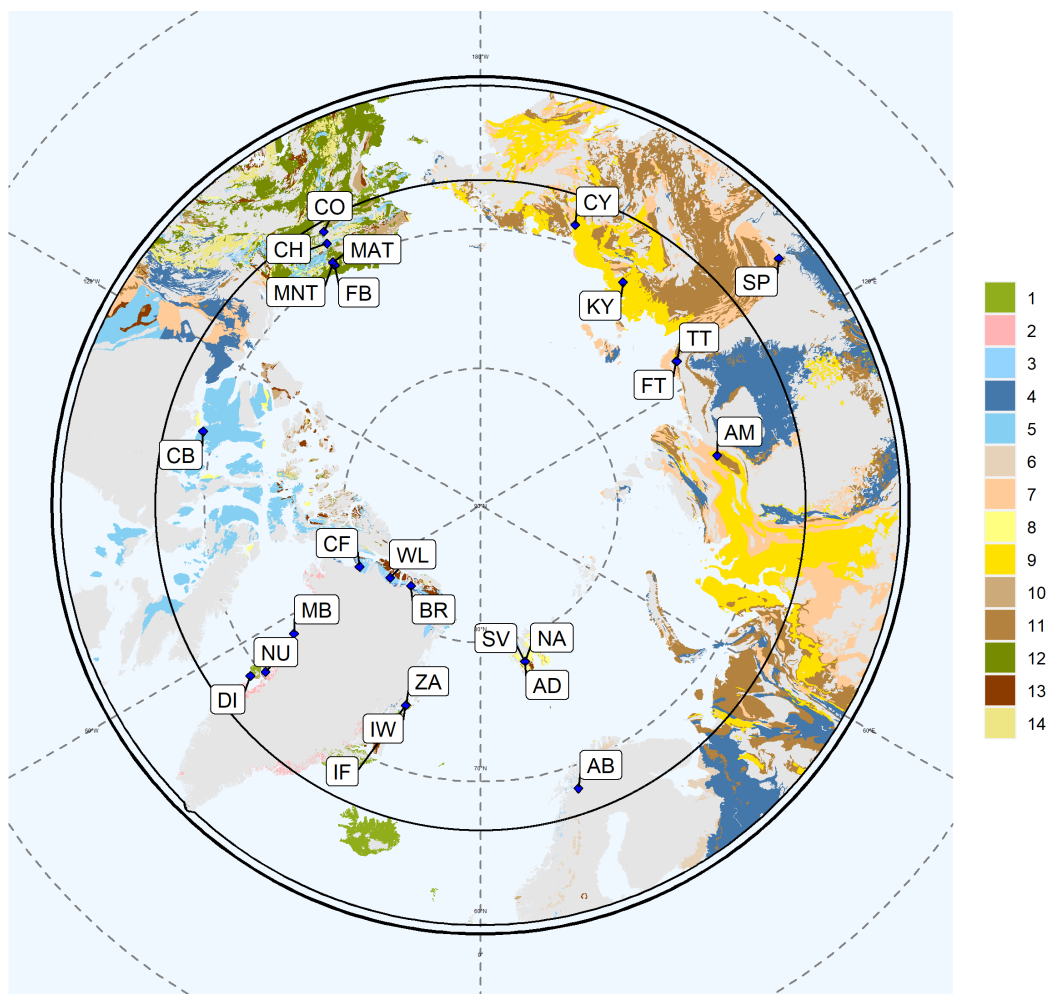
177

178

179 Fig. 1: Map of extrapolated element concentrations. The Arctic Circle (66.6°N) is included as a black circle. Each
180 color represents a bedrock lithology: 1: Basalt, olivine basalt, tholeiite, alkali basalt, basanite, pillow basalt, flood
181 basalt (n=26); 2: Gneiss, migmatite; reworked amphibolite and granulite facies rocks (n=11); 3: Limestone, dolostone,
182 shale, evaporites, chalk; carbonate reefs or metamorphosed equivalent (n=24); 4: Limestone, dolostone, shale,
183 evaporites, chalk; carbonate reefs; metamorphic grade not identified (n=58); 5: Limestone, dolostone, shale,
184 evaporites, chalk; carbonate reefs (n=64); 6: Quartz sandstone, siltstone, claystone, limestone, dolostone,
185 conglomerate, tillite (n=13); 7: Sandstone, siltstone, shale, coal; plant fossils; metamorphic grade not identified
186 (n=68); 8: Sandstone, siltstone, shale, limestone (n=38); 9: Sandstone, siltstone, shale, limestone; metamorphic grade

187 not identified (n=39); 10: Sandstone, siltstone, shale; marine fossils (n=91); 11: Sandstone, siltstone, shale; marine
188 fossils; metamorphic grade not identified (n=60); 12: Sedimentary and/or volcanic rock: undivided (n=21); 13: Shale,
189 chert, iron-formation, greywacke, turbidite, argillaceous limestone, matrix-supported conglomerate (n=43); 14: Shale,
190 chert, iron-formation, greywacke, turbidite, argillaceous limestone, matrix-supported conglomerate or
191 metamorphosed equivalent (n=8). Grey color means areas of base map that are not represented by our data on element
192 concentrations. Abbreviations for locations: CH: Alaska, Chandalar; CO: Alaska, Coldfoot; FB: Alaska, Franklin
193 Bluff-Dry; MAT: Alaska, Moist acidic tundra; MNT: Alaska, Moist non-acidic tundra; CB: Canada, Cambridge Bay;
194 BR: Greenland, Brønlund; CF: Greenland, Cass Fjord; DI: Greenland, Disko; MB: Greenland, Melville Bay; NU:
195 Greenland, Nussuaq; WL: Greenland, Warming Land; ZA: Greenland, Zackenberg; IW: Greenland, Zackenberg, Ice
196 Wedge; IF: Greenland, Zackenberg, Infilling Fan; AM: Russia, Ary-Mas; CY: Russia, Chersky; KY: Russia, Kytalyk;
197 FT: Russia, Lena delta, first terrace; TT: Russia, Lena Delta, third terrace; SP: Russia, Spasskaya; AB: Sweden,
198 Abisko; AD: Svalbard, Adventalen; NA: Svalbard, Adventalen; SV: Svalbard. This map is based on the Geological
199 Map of the Arctic (Harrison et al., 2011).
200

201   **3.2 Element availabilities across lithological classes at 0-1 m depth**

202   The lithological classes differed substantially in their element availabilities (Fig. 2; Fig S5):

203   • We found a large range in **ASi concentrations** in the Arctic covering values from 0.03±0 mg g^{-1} DW ASi to
204   6.68±1.17 mg g^{-1} DW ASi. The highest concentrations of ASi were found in basalt and associated rock (class 1:
205   6.68±1.17 mg g^{-1} DW ASi), Gneiss and associated rock (class 2: 4.11±1.24 mg g^{-1} DW ASi), Sandstone and
206   associated rock (class 9: 2.01±0.24 mg g^{-1} DW ASi. class 10: 2.06±0.01 mg g^{-1} DW ASi). ASi concentrations
207   were lowest in Limestone (class 3: 0.03±0 mg g^{-1} DW ASi) (Fig. 2).

208   • **Si concentrations** were highest in Limestone and associated rock including shale (class 4: 5.65±0.78 mg g^{-1} DW Si), Quartz sandstone (class 6: 6.61±1.83 mg g^{-1} DW Si) and Sandstone (class 7: 5.46±0.66 mg g^{-1} DW Si). Si concentrations were lowest in Limestone and associated rock (class 3: 0.1±0.02 mg g^{-1} DW Si)
209
210
211   (Fig. 2).

212   • The highest **Ca concentrations** were observed in Limestone and associated rock (class 3: 10.73±2.15 mg g^{-1} DW Ca), Sedimentary and/or volcanic rock (class 12: 8.77±0.12 mg g^{-1} DW Ca) and Sandstone and associated rock (class 8: 8.06±0.36 mg g^{-1} DW Ca). Ca concentrations were lowest in Gneiss (class 2: 0.05±0.02 mg g^{-1} DW Ca) (Fig. 2).
213
214
215

216   • **Fe concentrations** were highest in shale and associated rock (class 13: 2.93±0.45 mg g^{-1} DW Fe), Limestone
217   (class 4: 2.28±0.32 mg g^{-1} DW Fe) and Quartz sandstone (class 6: 2.49±0.69 mg g^{-1} DW Fe). The lowest Fe
218   concentrations were observed in lithological Limestone and associated rock (class 3: 0.01±0.001 mg g^{-1} DW Fe)
219   (Fig. 2).

220   • The highest **concentrations of Al** were observed in to quartz sandstone (class 6: 2.52±0.70 mg g^{-1} DW Al),
221   Sandstone (class 7: 1.63±0.20 mg g^{-1} DW Al) and shale and associated rock (class 13: 1.5±0.23 mg g^{-1} DW Al).
222   The lowest Al concentrations were observed in limestone and associated rock (class 3: 0.02±0 mg g^{-1} DW Al)
223   (Fig. 2).

224   • High **P concentrations** were observed in limestone and associated rock (class 4: 0.31±0.04 mg g^{-1} DW P),
225   Sandstone (class 7: 0.19±0.02 mg g^{-1} DW P) and Shale and associated rock (class 14: 0.15±0.05 mg g^{-1} DW P).
226   P concentrations were lowest in Basalt and associated rock (class 1: 0.0116±0.002 mg g-1 DW P) (Fig. 2).

227

228
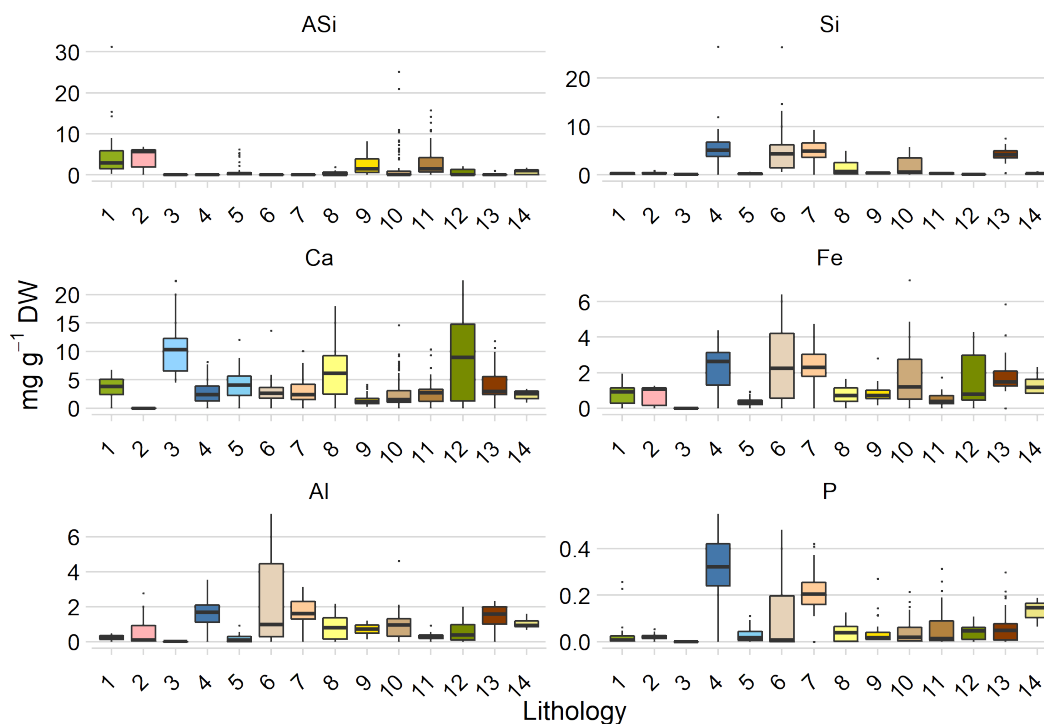
229

230 Fig. 2: Element concentrations related to lithology. Each color represents a bedrock lithology: 1: Basalt, olivine basalt,

231 tholeiite, alkali basalt, basanite, pillow basalt, flood basalt (n=26); 2: Gneiss, migmatite; reworked amphibolite and

232 granulite facies rocks (n=11); 3: Limestone, dolostone, shale, evaporites, chalk; carbonate reefs or metamorphosed

233 equivalent (n=24); 4: Limestone, dolostone, shale, evaporites, chalk; carbonate reefs; metamorphic grade not

234 identified (n=58); 5: Limestone, dolostone, shale, evaporites, chalk; carbonate reefs (n=64); 6: Quartz sandstone,

235 siltstone, claystone, limestone, dolostone, conglomerate, tillite (n=13); 7: Sandstone, siltstone, shale, coal; plant

236 fossils; metamorphic grade not identified (n=68); 8: Sandstone, siltstone, shale, limestone (n=38); 9: Sandstone,

237 siltstone, shale, limestone; metamorphic grade not identified (n=39); 10: Sandstone, siltstone, shale; marine fossils

238 (n=91); 11: Sandstone, siltstone, shale; marine fossils; metamorphic grade not identified (n=60); 12: Sedimentary

239 and/or volcanic rock: undivided (n=21); 13: Shale, chert, iron-formation, greywacke, turbidite, argillaceous limestone,

240 matrix-supported conglomerate (n=43); 14: Shale, chert, iron-formation, greywacke, turbidite, argillaceous limestone,

241 matrix-supported conglomerate or metamorphosed equivalent (n=8). All values are given in mean and standard error.

242 The distribution of the lithological classes is shown in Fig. 1, the assignment to the geographic domain is given in

243 Table S5.

244

3.3 Maps of element concentration in 1 m depth

3.3.1 Amorphous silica in top 1 m

We found the highest concentrations of ASi located in the Arctic-North Atlantic region (Fig. 3). Here, mafic basalt and metamorphic Gneiss are dominant (lithological class 1 and 2) and contained concentrations of 4.11±1.24 to 6.68±1.17 mg ASi g-1DW. Other high concentrations of ASi were found for the Brooks Range (Alaska), Chukotka, Arctic Shelf (eastern Siberia) and the West Siberian Basin. Those soil contained 2.01±0.24 mg ASi g-1 DW (lithological class 9). The Verkhoyansk-Kolyma region showed a lower concentration of 1.48±0.16 mg ASi g-1DW (lithological class 11). We found similar concentrations (1.24±0.14 mg ASi g-1DW; lithological class 5) were found for the Canadian Shield. We found low concentrations of 0.31±0.01 mg ASi g-1 DW (lithological class 12) in interior western Alaska and western parts of Brooks Range, Alaska, Chukotka and Arctic Shelf. Increasing active layer depth will potentially release higher ASi concentrations from permafrost soils (Fig. S6) in the Canadian Shield as the concentration in the permafrost layer is 2.80±2.50 mg ASi g-1DW (lithological class 5) compared to the 1.24±0.14 mg ASi g-1DW in the current active layer (Table S4). A further increase in ASi concentration can be expected for the Arctic, North-Atlantic region by permafrost thaw as the concentration is 8.68±2.51 mg ASi g-1DW in the permafrost layer compared to the 4.11±1.24 ASi g-1DW of the current active layer (lithological class 1) (Fig. S6 Table S4). However, the permafrost layer in Siberia contains lower concentrations of ASi (0.77±0.23 mg ASi g-1DW, lithological class 9 and 1.38±0.28 mg ASi g-1DW, lithological class 11) compared to current active layer with 2.01±0.24 mg ASi g-1DW (lithological class 9) and 1.48±0.16 mg ASi g-1DW (lithological class 11) probably leading to lower overall ASi concentrations with proceeding thaw.

265
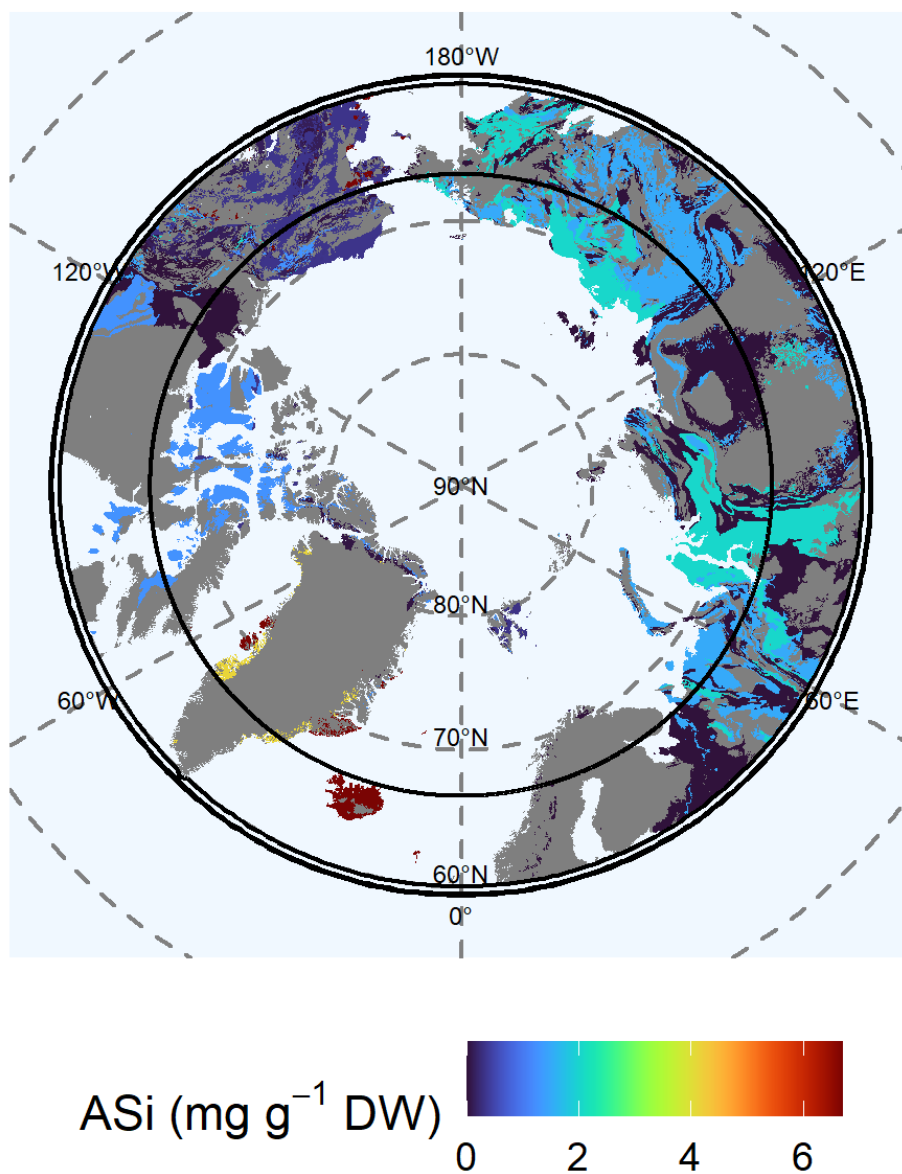
Fig. 3: Map of mean concentration of amorphous silica (ASi) in the top 100 cm of soils. For each lithological class
the mean concentration is shown. Grey shaded areas are not represented by our data.

- 13 -

268   **3.3.2 Silicon in 0-1 m depth**

269   Available Si (Fig. 4) showed a different distribution than ASi (Fig. 3). High Si concentrations were generally

270   associated with sediments. We found high concentrations (5.65 ± 0.78 mg Si g-1 DW) for lithological class 4, the

271   West Siberian basin and the Siberian plain. Other regions with high Si concentrations were the East European plain,

272   the Ural Mountains and the Canadian Shield. Another lithological class with high Si concentrations (4.51 ±

273   0.69 mg Si g-1 DW) is class 13, located in the Innutian Region, North Greenland and in Alaska. In Alaska lithological

274   class 10 with moderate high concentrations of Si (2.06 ± 0.03 mg Si g-1 DW) is also abundant. We found low

275   concentration of Si (0.36 ± 0.05 mg Si g-1 DW, lithological class 9) for Brooks Range, Chukotka, Arctic shelf, the

276   West Siberia Basin and the Siberian Plain. In addition, the Verkhoyansk-Kolyma-Region and the East-European Plain

277   and the Ural Mountains were poor in Si (0.39 ± 0.04 mg Si g-1 DW, lithological class 11). Lowest concentrations

278   (0.15 ± 0.01 mg Si g-1 DW, lithological class 12) were observed in Interior Western Alaska. Increasing thawing depth

279   may potentially increase Si concentrations in the western Verkhoyansk-Kolyma-Region to the east European Platform

280   as the concentration in the permafrost layer is 6.26±1.52 mg Si g-1DW (lithological class 4) compared to the lower Si

281   concentration of the current active layer with 5.56±0.78 mg Si g-1DW (lithological class 4) (Figure S6, Table S4).

282

283

284
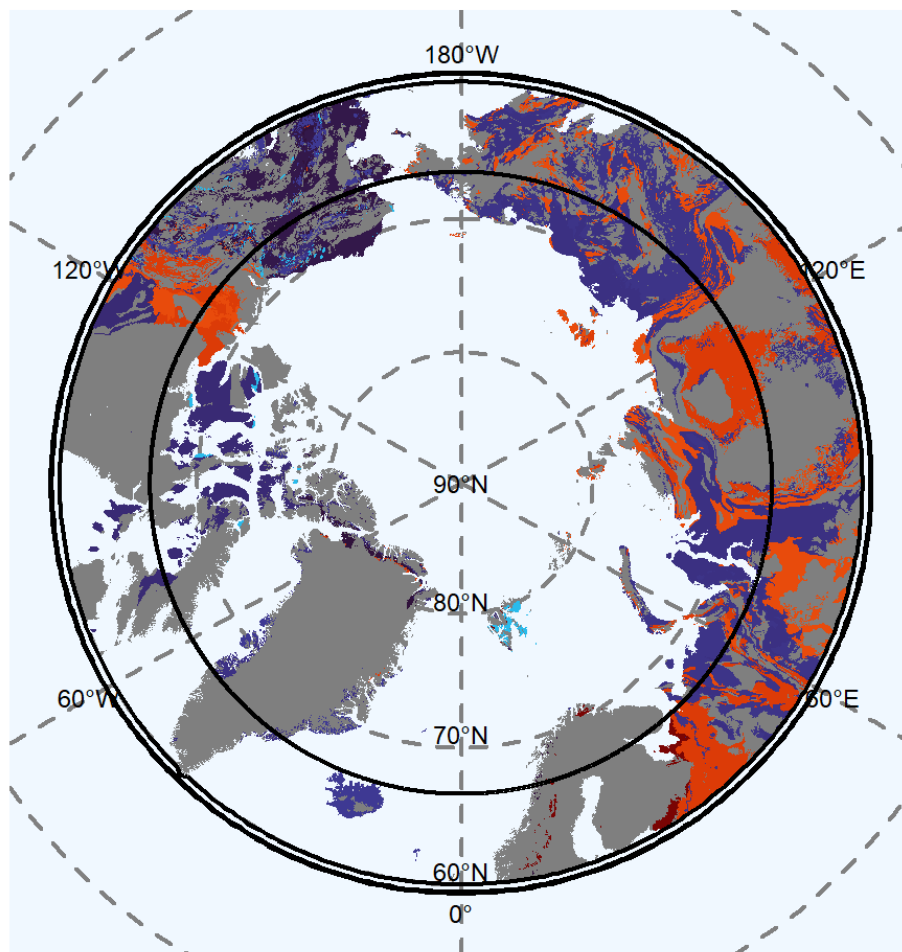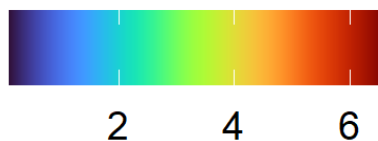
Fig. 4: Map of mean concentration of mineral silicon (Si) for the uppermost 100 cm of soils. For each lithological
class the mean concentration is shown. Blue colors represent low concentrations of Si; red colors represent high
concentrations. Grey shaded areas are not represented by our data.

3.3.3 Calcium in 0-1m depth

The highest Ca concentrations in soils was in limestone and associated rock (class 3: 10.73 ± 2.15 mg Ca g-1 DW) in North Greenland, Alaska and the Canadian Shield (3.79 ± 0.45 mg Ca g-1 DW, lithological class 5) (Fig. 5). In addition, supracrustal rocks in Alaska contained very high concentrations of Ca (8.77 ± 0.12 mg ca g-1 DW, lithological class 12). Mafic rocks in the Arctic North Atlantic region (3.65 ± 0.70 mg Ca g-1 DW, lithological class 1) contained moderate Ca concentrations. We found moderate to low Ca concentrations (2.88 ± 0.32 mg Ca g-1 DW, lithological class 11) for the soils of the Verkhoyansk-Kolyma-Region, the East European Plain and the Ural Mountains. Large regions of eastern and western Siberia and the Siberian Plain were poor in Ca (1.51 ± 0.14 mg Ca g-1 DW, lithological class 9; 2.56 ± 0.34 mg Ca g-1 DW, lithological class 4). The Ca concentrations of the permafrost layer for Alaska (10.42 ± 2.08 mg Ca g-1 DW, lithological class 12) is higher than in the active layer (2.93 ± 0.45 mg Ca g-1 DW) (Fig. S6). In the largest part of Siberia and the Canadian Shield the Ca concentrations are slightly lower in the permafrost layer with 2.15 ± 0.96 mg Ca g-1 DW (lithological class 4) and 1.59 ± 0.32 mg Ca g-1 DW, lithological class 7) than in the active layer with 2.56 ± 0.34 mg Ca g-1 DW (lithological class 4) and 1.51 ± 0.14 mg Ca g-1 DW, lithological class 7) (Figure S6, Table S4).

302
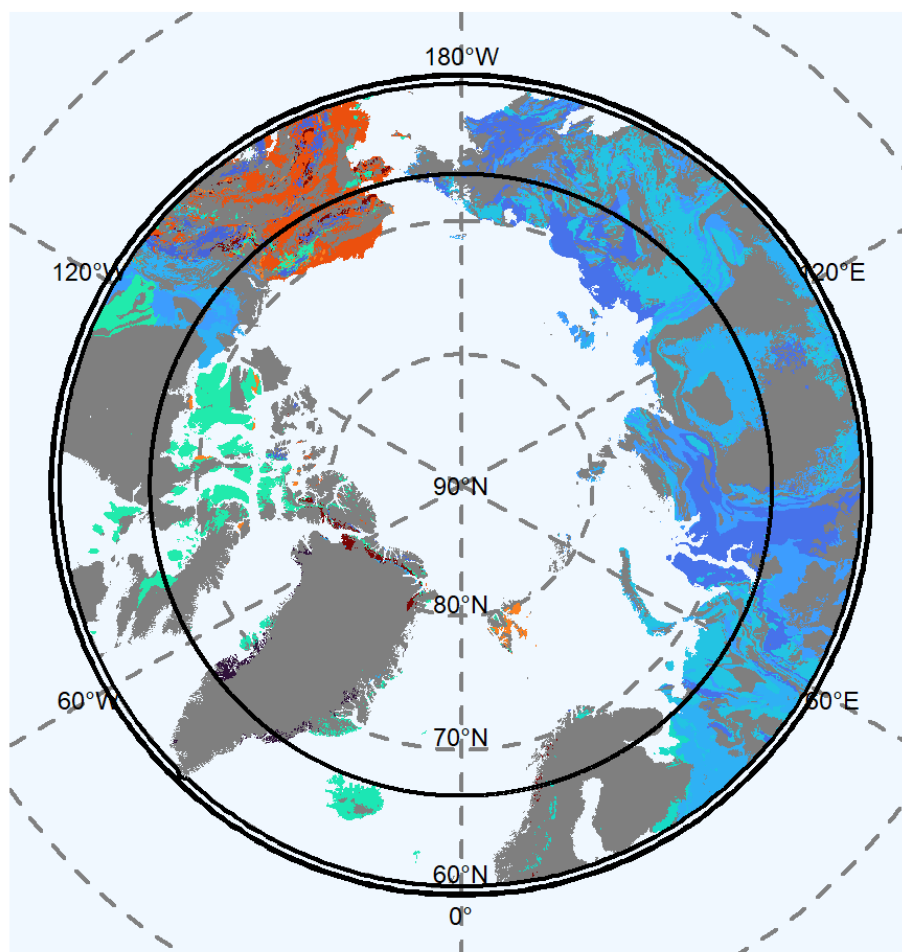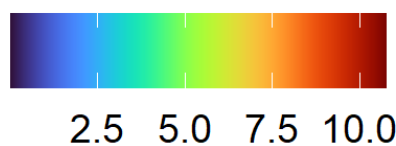
Fig. 5: Map of mean concentration of mineral calcium (Ca) for the uppermost 100 cm of soils. For each lithological
class the mean concentration is shown. Blue colors represent low concentrations of Ca, red colors represent high
concentrations. Grey shaded areas are not represented by our data.

306

3.3.4 Iron (Fe) in 0-1 m depth

Fe concentrations were higher in the eastern Arctic, than in the western Arctic (Fig. 6). We found highest concentrations in northern Greenland (lithological class 13 contained 2.93 ± 0.45 mg Fe g-1 DW). The soils of the lithological class 4 in the western Siberian Basin, Siberian and Canadian plain contained 2.28 ± 0.32 mg Fe g-1 DW. The Verkhoyansk-Kolyma region showed similar Fe concentrations (2.21 ± 0.27 mg Fe g-1 DW, lithological class 7). Moderate to high Fe concentration we found for igneous mafic rocks in Iceland and Greenland (0.94 ± 0.18 mg Fe g-1 DW, lithological class 1) and for supracrustal rocks in Alaska (1.24 ± 0.14 mg Fe g-1 DW, lithological class 12). The Chukotka region and western Siberia were relatively poor in Fe (0.83 ± 0.13 mg Fe g-1 DW, lithological class 9). Eastern Siberia and North Europe contained even lower Fe concentrations (0.49 ± 0.04 mg Fe g-1 DW, lithological class 11). Fe concentrations in the Canadian Shield were similarly low (0.41± 0.06 mg Fe g-1 DW, lithological class 12). We expect increasing Fe concentrations at the Canada and Greenland shield due to predicted future thaw of the permafrost layer as the concentration in the permafrost layer (0.61± 0.15 mg Fe g-1 DW, lithological class 5) and in parts of Alaska (1.97± 0.3 mg Fe g-1 DW, lithological class 14) is higher compared to the current active layer with (0.41± 0.05 mg Fe g-1 DW, lithological class 5) and in parts of Alaska (1.08± 0.38 mg Fe g-1 DW, lithological class 14) (Fig. S7, Table S4).

Fe (mg g^{-1} DW)   0.5 1.0 1.5 2.0
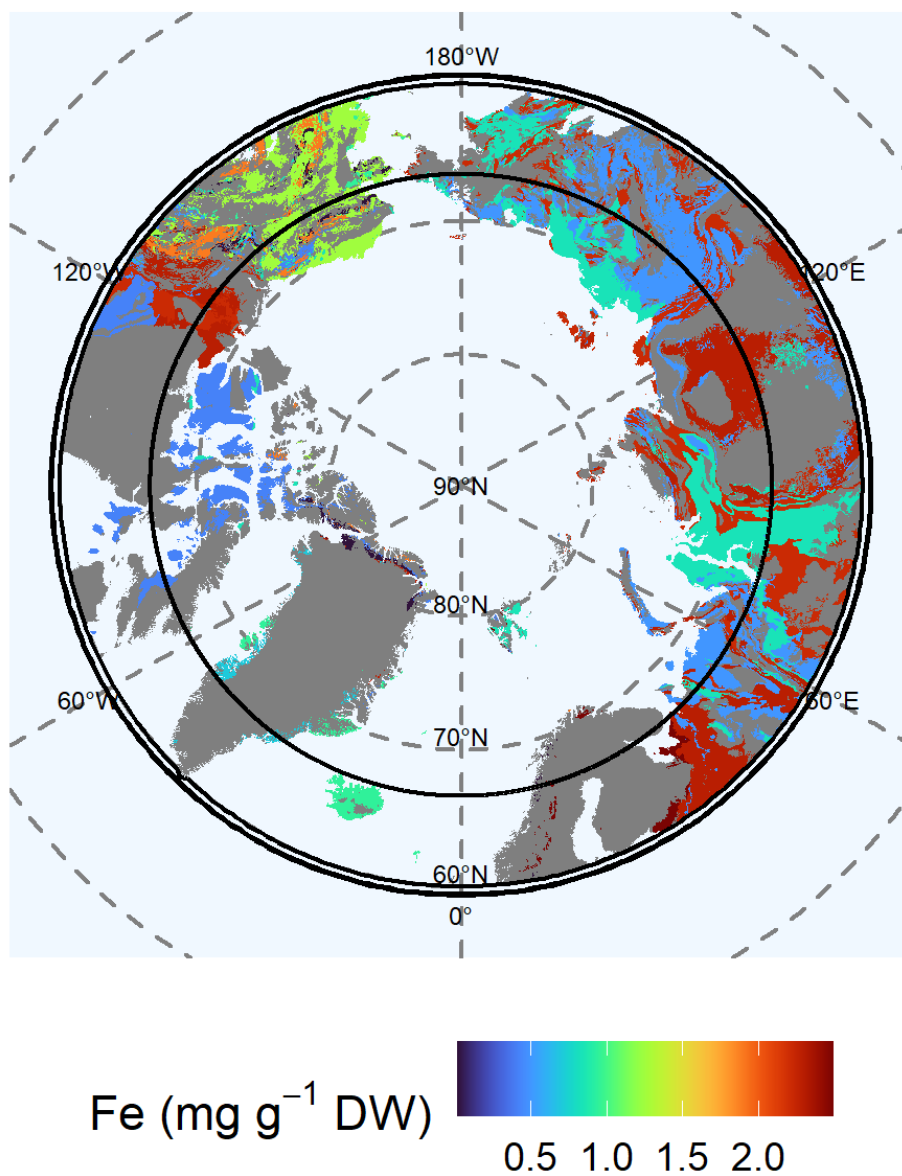
322

323   Fig. 6: Map of mean concentration of mineral iron (Fe) for the uppermost 100 cm of soils. For each lithological class
324   the mean concentration is shown. Blue colors represent low concentrations of Fe, red colors represent high
325   concentrations Grey shaded areas are not represented by our data.

3.3.5 Aluminum in 0-1 m depth

Northern Europe contained highest concentrations of available Al (2.52 ± 0.07 mg Al g-1 DW, lithological class 6) (Fig. 7). Relative high concentrations of Al were distributed over Siberia and the Canadian Shield (1.63 ± 0.02 mg Al g-1 DW, lithological class 7; 1.57 ± 0.22 mg Al g-1 DW lithological class 4). Parts of Alaska contained moderate Al concentrations (0.94 ± 0.06 mg Al g-1 DW, lithological class 10; 1.5 ± 0.23 mg Al g-1 DW, lithological class 13), while areas represented by supracrustal rocks were poor in Al (0.47 ± 0.06 mg Al g-1 DW, lithological class 12). We found relative low concentrations (0.73 ± 0.01 mg g-1 DW) of Al for Chukotka, eastern and western Siberia observed in lithological class 9. The Verkhoyansk-Kolyma Region and the East European plain showed the lowest Al concentrations (0.26 ± 0.02 mg Al g-1 DW, lithological class 11), together with the Canada plain (0.21 ± 0.03 mg g-1 DW Al, lithological class 5). Increasing thawing depth may increase the Al concentration by the predicted thaw of the permafrost layer in North Europe as the concentration in the permafrost layer is 4.88± 1.02 mg Al g-1 DW (lithological class 6) and across the Greenland and Canadian shield it is 0.3± 0.07 mg Al g-1 DW (lithological class 5) compared to the current active layer with 2.52± 0.7 mg Al g-1 DW (lithological class 6) and across the Greenland and Canadian shield it is 0.21± 0.03 mg Al g-1 DW (lithological class 5) (Fig. S7, Table S4).

340
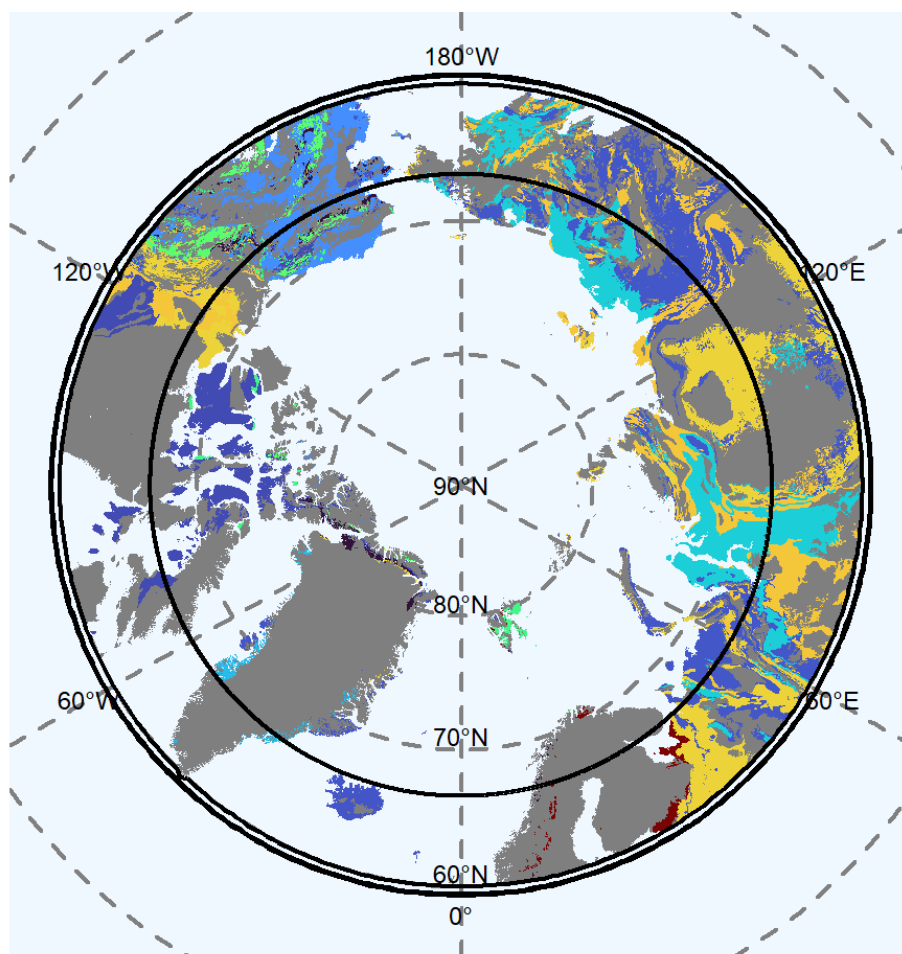
Fig. 7: Map of mean concentration of mineral aluminum (Al) for the uppermost 100 cm of soils. For each lithological class the mean concentration is shown. Blue colors represent low concentrations of Al, red colors represent high concentrations. Grey shaded areas are not represented by our data .

3.3.6 Phosphorous in 0-1 m depth

We found the highest P concentrations we found for the West Siberian Basin, the Canadian Shield and the Siberian and East European Plain (0.306 ± 0.042 mg P g-1 DW, lithological class 4) (Fig. 8). In the Chukotka region the P concentrations were 0.189 ± 0.023 mg P g-1 DW (lithological class 7. We found moderate P concentration for Northern Europe (0.123 ± 0.034 mg P g-1 DW, lithological class 6) and in Alaska (0.153± 0.054 mg P g-1 DW, lithological class 14). Wide areas of supracrustal rocks in Alaska were poor in P (0.024 ± 0.004 mg P g-1 DW, lithological class 12). The Canadian shield (0.037 ± 0.005 mg P g-1 DW, lithological class 5), the Verkhoyansk-Kolyma region, the east European Plain (0.017 ± 0.002 mg P g-1 DW, lithological class 11) and the Chukotka region (0.030 ± 0.003 mg P g-1 DW, lithological class 9) were poor in P. Due to permafrost thaw we expect increasing P concentrations the Canadian shield as the P concentrations in the permafrost layer is 0.06± 0.01 mg P g-1 DW (lithological class 5) compared to the current active layer with 0.04± 0.005 mg P g-1 DW (lithological class 5) (Fig. 7, Table S4).

356
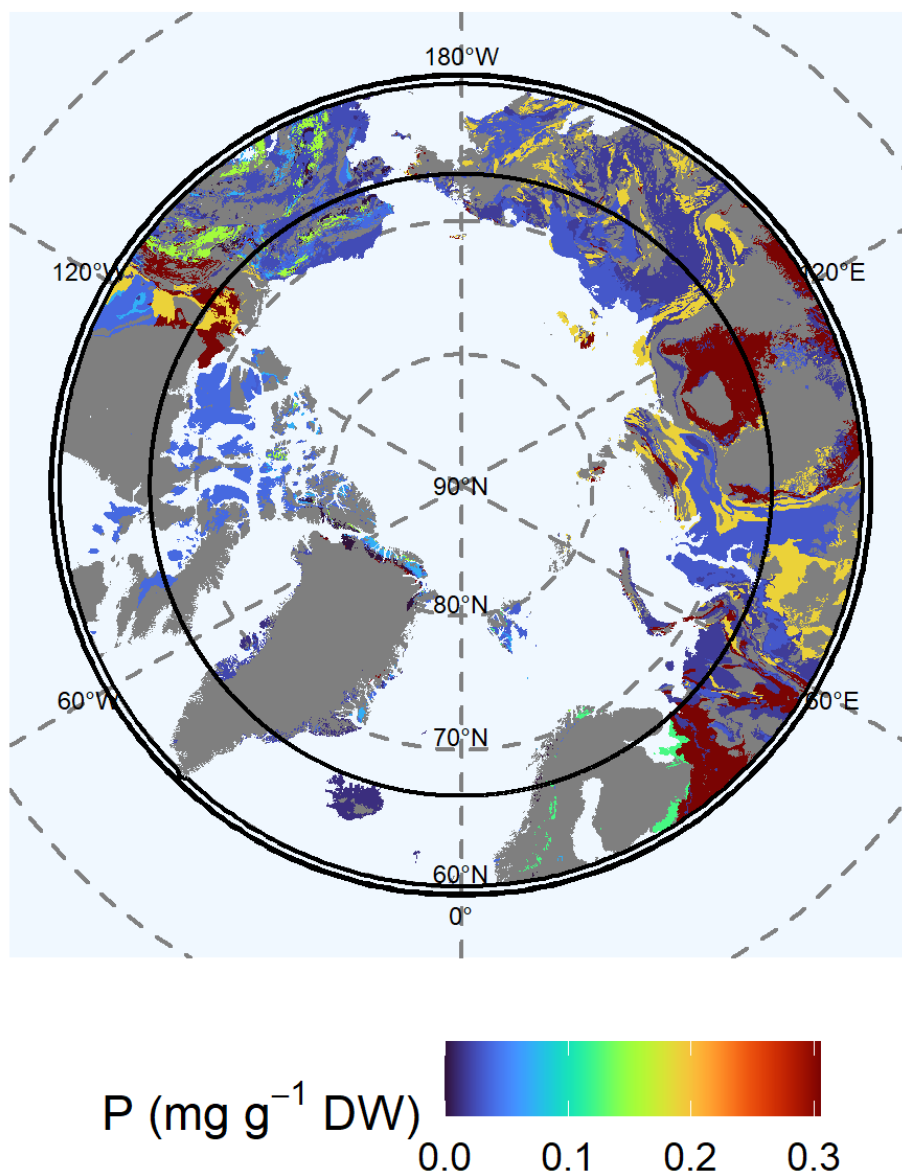
Fig. 8: Map of mean concentration of mineral phosphorous (P) for the uppermost 100 cm of soils. For each
lithological class the mean concentration is shown. Blue colors represent low concentrations of P, red colors
represent high concentrations. Grey shaded areas are not represented by our data .

4 Discussion

4.1 Element availability in relation to lithology and geography

We found large differences in the availability of all analysed elements between the different lithology classes of the Arctic. The igneous lithological type for example is dominated by alkaline and Ca-rich basaltic rocks from Alaska. Rocks built up by sedimentation are often more complex or variable in their chemical composition than igneous rocks. Sedimentary rocks cover a wide range of pH, as the parent material is more diverse. Limestone sediments for example differ in their content of Fe and P, depending if their origin is biological (lithological class 4), physical or chemical. Sandstone can contain high Fe concentrations, too, but it contains Si as the main element (lithological class 7-8) (Yurchenko et al., 2019). Previously, there was no map existing for availability of Si, Ca, Fe, P, and Al in Arctic soils, and only a map on ASi stocks but not concentrations. Our maps show element concentration available for plants and microbes together. We further show what changes in element availability will occur during permafrost thaw and we discuss these changes in element availability in regard to occurring nutrient limitations and Arctic C-fluxes.

4.2 Relevance of element availability in a dynamic Arctic

Low temperatures in the Arctic systems slow down biological and chemical processes and preserve OM for millennia (Sher et al., 2005). Due to Arctic warming these processes are accelerated by an increased nutrient and OM mobilization from the permafrost (Salmon et al., 2016). Consequently, OM may become vulnerable to respiration (Hugelius et al., 2020; Strauss et al., 2017). However, OM is not the single driving force regarding the acceleration of Arctic soil respiration. Elements like Si, Ca, Fe, P and Al may also interfere this process (Monhonval et al., 2021a; Monhonval et al., 2021b).

Nutrient cycles and limitations were identified as important for improving of high latitude ecosystems estimations vegetation functional parameter like gross primary production (GPP) (Chadburn et al., 2017). The dataset presented in our study could therefore serve as a basis for providing soil nutrient concentrations for biogeochemical models that are capable of considering nutrient limitations in permafrost ecosystems. Our maps cover nearly the half of the Arctic area. The distribution of ASi in Arctic regions was first estimated by Alfredsson et al. (2016). Alfredsson et al. (2016) showed maps of ASi stocks (not concentrations) related to vegetation cover, covering 30 soil profiles. The effect of current vegetation on mineral availability in soils is low and associated with high uncertainties as the vegetation involved in forming the soil ASi pool may be different. A more appropriate measure of element availability may be parent material and lithology (Alloway, 2013). It was shown, that geochemical element concentration in Arctic permafrost soil allow to distinguish geologies (Reimann and Melezhik, 2001). Consequently, our lithology-based extrapolation of nutrient availability will help to reduce the so far uncertainties in pan-Arctic soil element availability. Due to deepening of the active layer, as for example observed at the Canadian shield and in the North-Atlantic region, our data suggest higher ASi concentrations, as the concentration in the permafrost layer is higher compared to shallower soil layers (Fig. S6). This may increase P and OM availability (Reithmaier et al., 2017; Schaller et al., 2019) by competing for binding sites on the surface of minerals subsequently mobilizing both P and OM, potentially increasing the leaching of both to the sea. It was also shown that Si leads to a release of P from minerals of Arctic

396 soils and increases OM decomposition, increasing soil greenhouse gas release (Schaller et al., 2019). Ca can
397 immobilize OM by cation bridging and by this preserve OM from microbial decomposition (Sowers et al., 2020). Ca
398 reduces the osmotic stress for microbes (Läuchli and Grattan, 2007) by decreasing the freezing point of water and
399 increasing the availability of liquid pore water (Jessen et al., 2014). Ca is relevant for the mineral formation because
400 it can bind CO_2 as $Ca(HCO_3)_2$ in soil with pH higher than 7 (Dessert et al., 2003; Köhler et al., 2010). The
401 concentration of soluble Ca in Yedoma soils is mainly driven by thermokarst processes. In deeper soil layers, Ca
402 concentrations are usually lower than in upper layers. Consequently, a future increase in temperatures may lead to a
403 widespread decrease in Ca concentrations, especially in the Yedoma regions. Fe is also of high importance for
404 ecosystems as it is a key element in microbial activity (Colombo et al., 2014) and nitrogen fixation (Jasniewski et al.,
405 2019). Fe minerals are important electron acceptors under anaerobic conditions and Fe is essential for microbial
406 methane production (Colombo et al., 2018). After being released from rocks by weathering, Al forms amorphous
407 aluminosilicates that mineralizes slowly (Schaller et al., 2021). Al is relevant for the OM respiration due to its high
408 cytotoxicity to organisms (Rengel, 2004). Thawing permafrost may be a source for Al, especially across Canada, the
409 Greenland shield and Northern Europe. Increasing P availability, as predicted for Greenland and the Canadian shield
410 (Fig. 7) may for example increase CO_2 release to the atmosphere by increasing the mineralization rates of OM (Street
411 et al., 2018; Yang et al., 2021).

4.3 Importance of element interactions for nutrient availability

414 In permafrost layers, the mineralization of OM by microbial activity is negligible due to frozen conditions. Like in
415 temperate soils, binding of OM on mineral phases can prevent OM from mineralization (Dutta et al., 2006; Mueller et
416 al., 2015). Mineral phases may bind parts of soil OM reducing the amount of OM for microbial respiration. A large
417 share of OM may be associated with iron and aluminium oxides/hydroxides. In particular iron minerals may strongly
418 bind OM, whereby a high stability of stored carbon is likely (Herndon et al., 2017). Thereby the binding between OM
419 and the minerals is determined by the quantity of minerals that can bind OM (Wiseman and Püttmann, 2006). This
420 would imply that a higher concentration of Fe, Al and Ca in Arctic soils due to permafrost thaw may lead to a lower
421 GHG emission from Arctic soils due to complexation of OM with those elements. Such increase in element availability
422 binding OM and with this resulting in potentially lower GHG emissions may happen for Alaska (higher Ca and Fe
423 concentration in permafrost layer compared to current active layer), Canadian Shield and Greenland (higher Fe and
424 Al concentration in permafrost layer compared to current active layer), and North Europe (higher Al concentration in
425 permafrost layer compared to current active layer) (see results part). However, lower Ca concentrations can be
426 expected in large parts of Siberia and the Canadian Shield, as the concentrations in the permafrost layer are lower
427 compared to the current active layer. Si however, can potentially mobilize OM from those phases, by binding
428 competition of silicic acid with some functional groups of organic material (Hömberg et al., 2020), potentially
429 increasing GHG emssions. An increase in Si availability upon permafrost thaw can be expected in the western
430 Verkhoyansk-Kolyma-Region to the east European Platform as the concentration in the permafrost layer is higher
431 compared to the current active layer (see results part). P competes with OM for binding on soil minerals (Schneider

432   et al., 2010). Such increasing P concentration due to permafrost thaw can be expected for the Canadian Shield (results

433   part). Based on the differences in element (Si, Fe, Al, Ca and P) concentration, the stability of OM differs in Arctic

434   regions, depending on the dominating mineral composition, lithology and element availability. Also the availability

435   of nutrients (P in this case) is modified by mineral composition. For example, P is often strongly bound to Fe mineral

436   phases, reducing P availability (Gérard, 2016). Si however, is able to mobilize P from strong binding to Fe mineral by

437   competing for binding sites (Schaller et al., 2019). Unlike Si, Ca binds P by calcium phosphate precipitation at alkaline

438   conditions (Cao and Harris, 2008) or as calcium carbonate/phosphate co-precipitation (Otsuki and Wetzel, 1972).

439   Under conditions of low Fe availability in soils, the binding of P may be related to Al-minerals (Eriksson et al., 2015).

440   A lack of available P leads also to a reduction of the physiological activity of microbes (Walker et al., 2001), thus

441   potentially reducing microbial respiration of OM. Free Si seems limit the availability of ions like Fe, Al, or Ca by

442   precipitating those elements in amorphous or crystalline phases (Schaller et al., 2021). Hence, the mobilization of

443   elements like Si, Ca, Fe and Al strongly interfere with both P and OM availability and thus potentially with GHG

444   emissions. To unravel the dominant processes upon permafrost thaw, or which element mobilization is dominant in

445   terms of OM binding or mobilization and with this affecting GHG emission, future studies are urgently needed.

446

4.4 Transport of elements to the Arctic Ocean

448   With the ongoing deepening of the active layer in Arctic soils, an increased leaching of elements and nutrients may

449   occur (Mann et al., 2022; Sanders et al., 2022), which may substantially impact marine biodiversity and ecosystem

450   function. We have shown for several regions of the Arctic that there will be regional differences in element

451   mobilization upon permafrost thaw. For example, increased export of Fe and P, which are the main limiting nutrients

452   for marine net primary production (NPP; Zabel and Schulz (2006)), has already contributed to a 30% increase in NPP

453   in the Arctic Ocean between 1998 and 2009 (Arrigo and van Dijken, 2011). Increased Fe concentration upon

454   permafrost thaw can be expected for the Canadian Shield, Greenland and Alaska, whereas increased P mobilization

455   may occur only in the Canadian Shield. Si and Ca also have a crucial role in marine primary production. Both elements

456   are components of the inorganic spheres of diatoms (Si) and coccolithophores (Ca), which fix CO_2 in the Arctic

457   Ocean, an important global carbon sink (Krause et al., 2018). At the Arctic Canadian coast, Si inputs led to an increase

458   of diatoms from 2 % to 37 % (Terhaar et al., 2021). Diatoms and coccolithophores are the basis of the marine food

459   chain, and therefore, shifts in their populations may have widespread implications for the marine ecosystem (Daniels

460   et al., 2018). Permafrost thaw is likely to accelerate inputs of Si and Ca to Arctic waters. Increased Si concentration

461   can be expected in the western Verkhoyansk-Kolyma-Region to the east European Platform as the concentration in

462   the permafrost layer is higher compared to the current active layer, (see Results section). Ca mobilization may increase

463   or decrease depending on the Arctic region. Increase Ca mobilization can be expected for Alaska, whereas a slight

464   decrease in Ca mobilization may occur in large parts of Siberia and the Canadian Shield (see Results section). Yedoma

465   deposits readily leach soluble ions, including Si and Ca, as a result of thaw degradation (Strauss et al., 2017). Alaskan

466   soils store huge amounts of Ca in the mineral layer (see above) that could be transported to the Beringia Sea with

467   increasing soil degradation, promoting the growth of coccolithophores. In Siberia, the Lena River could transport large

468 amounts of Si to the Laptev Sea increasing the growth of diatoms. The same could happen at the East European plain.
469 In the same way P concentrations in these regions of the Arctic Sea could rise, too, as P concentrations in the
470 permafrost layer of the Canadian Shield are higher compared with the current active layer (see results part). In
471 summary, in the many areas of the Arctic with high Si, Ca and P storage, there could be increased inputs to Arctic
472 waters with permafrost thaw potentially increasing CO_2 fixation by marine primary production.
473

474 **5 Data availability**

475 The data for element availability from all single locations, soil profiles, transects, lithology's, as well as bootstrap data
476 for location and lithology can be can be downloaded via the open-access MPG repository EDMONT under
477 https://doi.org/10.17617/3.8KGQUN (Schaller and Göckede, 2022). During review process, the data is available
478 under: https://edmond.mpdl.mpg.de/privateurl.xhtml?token=8cbb0bd8-790f-4719-8cd1-a3df4ff99477 (Schaller and
479 Göckede, 2022) to allow corrections based on reviewer comments. The repository contains a readme file ("Read
480 me.docx"). In this file, all necessary information can be found, including all columns descriptions need to use the data.
481 The element availability from all single locations, soil profiles, transects, lithology's labelled (loction_samples.txt)
482 with following parameters: geological map of the Arctic, individual ID of the polygon, official name of the sampling
483 site, study internal name of the soil sample, soil horizon, coordinates of sampling sites, concentration of alkaline
484 extractable silicon, Mehlich-3 extractable Si, Ca, Fe Al and P, thickness of the layer, original depth where soil was
485 taken, size of the polygon that contains the sampling site, age code, scientific name of the age, where bedrock was
486 formed, scientific name of the eon, where bedrock was formed, scientific name of the era, where bedrock was formed,
487 scientific name of the period, where bedrock was formed, maximal and minimal age of bedrock, information if
488 lithogenesis was of the supracrustal, sedimentary or igneous type, most common rock types in the cluster group of the
489 setting, code of metamorphic type, code of domain region, name of tectonic and geographic domain, as well as name
490 of region within geographic domain.
491 In the location_bootstrap.txt file the bootstrapped means of concentration of alkaline extractable silicon, Mehlich-3
492 extractable Si, Ca, Fe Al and P for the organic, mineral active and permafrost layer of the single locations are given
493 in mg/g DW.
494 In the file "lithology_bootstrap.txt" element concentration for the first 1 m, including organic, mineral and permafrost
495 layer are given as bootstrapped mean with standard deviation for alkaline extractable silicon as well as Mehlich-3
496 extractable Si, Ca, Fe Al and P.
497

498 **6 Conclusion**

499 Here, we identified large differences in Si, Ca, Fe, P, and Al availability between different Arctic regions. With the
500 future projected warming of the Arctic and the associated thaw of permafrost, the availabilities of the elements will
501 change. Depending on dominance or limitation of certain elements, biogeochemical processes such as OM
502 mineralization may increase or decrease. Moreover, not only microbial processes like OM respiration may be affected

503   by changes in Si, Ca, Fe, P, and Al availability, but also processes such as primary production (CO_2 fixation by plants)

504   in terrestrial systems. This could be stabilizing soil OM, but may also trigger elevated biomass production of plants

505   due to increased nutrient supply. In addition, marine systems will receive higher loads of leached elements, which

506   could increase algae biomass production due to larger nutrient transport to the sea. Our spatially data product including

507   the differences in elements availability between the different lithological classes and regions will help improving

508   models of Arctic biogeochemical cycles for estimating future carbon feedback under the predicted climate change.

509

512

513   **Acknowledgments.** We thank Mrs. Lidia Völker (ZALF) for help with data extraction from the GIS polygons.

514

515   **Financial support.** The work was funded by the German Research Foundation (DFG), grant number SCHA 1822/12-

516   1 to Jörg Schaller. J. Strauss work was embedded into the 'Changing Arctic Ocean (CAO)' program (CACOON

517   project [#03F0806A (BMBF)]. Grant NSF-1417700 to SMN.

518

References

Abbott, B. W., Jones, J. B., Godsey, S. E., Larouche, J. R., and Bowden, W. B.: Patterns and persistence of hydrologic carbon and nutrient export from collapsing upland permafrost, Biogeosciences, 12, 3725-3740, 2015.

Alfredsson, H., Clymans, W., Hugelius, G., Kuhry, P., and Conley, D. J.: Estimated storage of amorphous silica (ASi) in soils of the circum-Arctic tundra region, Glob. Biogeochem. Cycle, 30, 479–500, 2016.

Alloway, B. J.: Bioavailability of elements in soil. In: Essentials of medical geology, Springer, 2013.

Arrigo, K. R. and van Dijken, G. L.: Secular trends in Arctic Ocean net primary production, Journal of Geophysical Research: Oceans, 116, 2011.

Box, J. E., Colgan, W. T., Christensen, T. R., Schmidt, N. M., Lund, M., Parmentier, F.-J. W., Brown, R., Bhatt, U. S., Euskirchen, E. S., and Romanovsky, V. E.: Key indicators of Arctic climate change: 1971–2017, Environ. Res. Lett., 14, 045010, 2019.

Brady, N. C. and Weil, R. R.: The nature and properties of soils, Prentice Hall Upper Saddle River, NJ, 2008.

Brown, J. and Romanovsky, V. E.: Report from the International Permafrost Association: State of permafrost in the first decade of the 21st century, Permafrost and Periglacial Processess. 19 (2): 255-260, 2008. 2008.

Cao, X. and Harris, W.: Carbonate and magnesium interactive effect on calcium phosphate precipitation, Environ. Sci. Technol., 42, 436-442, 2008.

Chadburn, S. E., Krinner, G., Porada, P., Bartsch, A., Beer, C., Belelli Marchesini, L., Boike, J., Ekici, A., Elberling, B., and Friborg, T.: Carbon stocks and fluxes in the high latitudes: using site-level data to evaluate Earth system models, Biogeosciences, 14, 5143-5169, 2017.

Colombo, C., Palumbo, G., He, J.-Z., Pinton, R., and Cesco, S.: Review on iron availability in soil: interaction of Fe minerals, plants, and microbes, Journal of soils and sediments, 14, 538-548, 2014.

Colombo, N., Salerno, F., Gruber, S., Freppaz, M., Williams, M., Fratianni, S., and Giardino, M.: Impacts of permafrost degradation on inorganic chemistry of surface fresh water, Global and Planetary change, 162, 69-83, 2018.

Daniels, C. J., Poulton, A. J., Balch, W. M., Marañón, E., Adey, T., Bowler, B. C., Cermeño, P., Charalampopoulou, A., Crawford, D. W., and Drapeau, D.: A global compilation of coccolithophore calcification rates, Earth System Science Data, 10, 1859-1876, 2018.

DeMaster, D. J.: The supply and accumulation of silica in the marine environment, Geochim. Cosmochim. Acta, 45, 1715-1732, 1981.

Dessert, C., Dupré, B., Gaillardet, J., François, L. M., and Allegre, C. J.: Basalt weathering laws and the impact of basalt weathering on the global carbon cycle, Chem. Geol., 202, 257-273, 2003.

Dutta, K., Schuur, E., Neff, J., and Zimov, S.: Potential carbon release from permafrost soils of Northeastern Siberia, Glob. Change Biol., 12, 2336-2351, 2006.

Eriksson, A. K., Gustafsson, J. P., and Hesterberg, D.: Phosphorus speciation of clay fractions from long-term fertility experiments in Sweden, Geoderma, 241, 68-74, 2015.

555 Faucherre, S., Jørgensen, C. J., Blok, D., Weiss, N., Siewert, M. B., Bang-Andreasen, T., Hugelius, G., Kuhry, P.,
556   and Elberling, B.: Short and long-term controls on active layer and permafrost carbon turnover across the
557   Arctic, Biogeosciences, doi: 10.1002/2017JG004069, 2018. 2018.

558 Fuchs, M., Grosse, G., Strauss, J., Günther, F., Grigoriev, M., Maximov, G. M., and Hugelius, G.: Carbon and
559   nitrogen pools in thermokarst-affected permafrost landscapes in Arctic Siberia, Biogeosciences, 15, 953-971,
560   2018.

561 Gérard, F.: Clay minerals, iron/aluminum oxides, and their contribution to phosphate sorption in soils—A myth
562   revisited, Geoderma, 262, 213-226, 2016.

563 Harrison, C., St-Onge, M., Petrov, O., Strelnikov, S., Lopatin, B., Wilson, F., Tella, S., Paul, D., Lynds, T., and
564   Shokalsky, S.: A new geological map of the Arctic, 2011, 750-752.

565 Herndon, E., AlBashaireh, A., Singer, D., Chowdhury, T. R., Gu, B., and Graham, D.: Influence of iron redox
566   cycling on organo-mineral associations in Arctic tundra soil, Geochim. Cosmochim. Acta, 207, 210-231,
567   2017.

568 Holmes, R. M., Coe, M. T., Fiske, G. J., Gurtovaya, T., McClelland, J. W., Shiklomanov, A. I., Spencer, R. G.,
569   Tank, S. E., and Zhulidov, A. V.: Climate change impacts on the hydrology and biogeochemistry of Arctic
570   rivers, Climatic change and global warming of inland waters, 2013. 1-26, 2013.

571 Hömberg, A., Obst, M., Knorr, K.-H., Kalbitz, K., and Schaller, J.: Increased silicon concentration in fen peat leads
572   to a release of iron and phosphate and changes in the composition of dissolved organic matter, Geoderma,
573   374, 114422, 2020.

574 Hugelius, G., Loisel, J., Chadburn, S., Jackson, R. B., Jones, M., MacDonald, G., Marushchak, M., Olefeldt, D.,
575   Packalen, M., and Siewert, M. B.: Large stocks of peatland carbon and nitrogen are vulnerable to permafrost
576   thaw, Proceedings of the National Academy of Sciences, 117, 20438-20446, 2020.

577 Hugelius, G., Strauss, J., Zubrzycki, S., Harden, J. W., Schuur, E., Ping, C.-L., Schirrmeister, L., Grosse, G.,
578   Michaelson, G. J., and Koven, C. D.: Estimated stocks of circumpolar permafrost carbon with quantified
579   uncertainty ranges and identified data gaps, Biogeosciences, 11, 6573-6593, 2014.

580 IPCC: Climate Change 2021: The Physical Science Basis. Contribution of Working Group I to the Sixth Assessment
581   Report of the Intergovernmental Panel on Climate Change. Climate Change., 236 pp., 2021.

582 Jasniewski, A. J., Wilcoxen, J., Tanifuji, K., Hedman, B., Hodgson, K. O., Britt, R. D., Hu, Y., and Ribbe, M. W.:
583   Spectroscopic Characterization of an Eight-Iron Nitrogenase Cofactor Precursor that Lacks the "9th Sulfur",
584   Angewandte Chemie, 131, 14845-14849, 2019.

585 Jessen, S., Holmslykke, H. D., Rasmussen, K., Richardt, N., and Holm, P. E.: Hydrology and pore water chemistry
586   in a permafrost wetland, Ilulissat, Greenland, Water resources research, 50, 4760-4774, 2014.

587 Kaiser, K. and Zech, W.: Competitive sorption of dissolved organic matter fractions to soils and related mineral
588   phases, Soil Sci. Soc. Am. J., 61, 64-69, 1997.

589 Köhler, P., Hartmann, J., and Wolf-Gladrow, D. A.: Geoengineering potential of artificially enhanced silicate
590   weathering of olivine, Proc. Natl. Acad. Sci. U. S. A., 107, 20228-20233, 2010.

591 Krause, J. W., Duarte, C. M., Marquez, I. A., Assmy, P., Fernández-Méndez, M., Wiedmann, I., Wassmann, P.,
592   Kristiansen, S., and Agustí, S.: Biogenic silica production and diatom dynamics in the Svalbard region during
593   spring, Biogeosciences, 15, 6503-6517, 2018.

594 Kuhry, P., Bárta, J., Blok, D., Elberling, B., Faucherre, S., Hugelius, G., Jørgensen, C. J., Richter, A., Šantrůčková,
595   H., and Weiss, N.: Lability classification of soil organic matter in the northern permafrost region,
596   Biogeosciences, 17, 361-379, 2020.

597 Läuchli, A. and Grattan, S.: Plant growth and development under salinity stress. In: Advances in molecular breeding
598   toward drought and salt tolerant crops, Springer, 2007.

599 Mann, P. J., Strauss, J., Palmtag, J., Dowdy, K., Ogneva, O., Fuchs, M., Bedington, M., Torres, R., Polimene, L.,
600   and Overduin, P.: Degrading permafrost river catchments and their impact on Arctic Ocean nearshore
601   processes, Ambio, 51, 439-455, 2022.

602 Mishra, U., Hugelius, G., Shelef, E., Yang, Y., Strauss, J., Lupachev, A., Harden, J. W., Jastrow, J. D., Ping, C.-L.,
603   Riley, W. J., Schuur, E. A. G., Matamala, R., Siewert, M., Nave, L. E., Koven, C. D., Fuchs, M., Palmtag, J.,
604   Kuhry, P., Treat, C. C., Zubrzycki, S., Hoffman, F. M., Elberling, B., Camill, P., Veremeeva, A., and Orr, A.:
605   Spatial heterogeneity and environmental predictors of permafrost region soil organic carbon stocks, Science
606   Advances, 7, eaaz5236, 2021.

607 Monhonval, A., Mauclet, E., Pereira, B., Vandeuren, A., Strauss, J., Grosse, G., Schirrmeister, L., Fuchs, M., Kuhry,
608   P., and Opfergelt, S.: Mineral element stocks in the Yedoma domain: a novel method applied to ice-rich
609   permafrost regions, Frontiers in Earth Science, 9, 2021a.

610 Monhonval, A., Strauss, J., Mauclet, E., Hirst, C., Bemelmans, N., Grosse, G., Schirrmeister, L., Fuchs, M., and
611   Opfergelt, S.: Iron redistribution upon thermokarst processes in the Yedoma domain, Frontiers in Earth
612   Science, 9, 2021b.

613 Mueller, C. W., Rethemeyer, J., Kao-Kniffin, J., Löppmann, S., Hinkel, K. M., and G. Bockheim, J.: Large amounts
614   of labile organic carbon in permafrost soils of northern A laska, Glob. Change Biol., 21, 2804-2817, 2015.

615 Otsuki, A. and Wetzel, R. G.: Coprecipitation of phosphate with carbonates in a marl lake, Limnol. Oceanogr., 17,
616   763-767, 1972.

617 Quideau, S., Chadwick, O., Trumbore, S. E., Johnson-Maynard, J., Graham, R., and Anderson, M.: Vegetation
618   control on soil organic matter dynamics, Org. Geochem., 32, 247-252, 2001.

619 R_Core_Team: R: A language and environment for statistical computing, 2021. 2021.

620 Reimann, C. and Melezhik, V.: Metallogenic provinces, geochemical provinces and regional geology—what causes
621   large-scale patterns in low density geochemical maps of the C-horizon of podzols in Arctic Europe?, Appl.
622   Geochem., 16, 963-983, 2001.

623 Reithmaier, G. M. S., Knorr, K. H., Arnhold, S., Planer-Friedrich, B., and Schaller, J.: Enhanced silicon availability
624   leads to increased methane production, nutrient and toxicant mobility in peatlands, Scientific Reports, 7,
625   8728, 2017.

626 Rengel, Z.: Aluminium cycling in the soil-plant-animal-human continuum, Biometals, 17, 669-689, 2004.

627 Romanovsky, V. E., Drozdov, D., Oberman, N. G., Malkova, G., Kholodov, A. L., Marchenko, S., Moskalenko, N.
628   G., Sergeev, D., Ukraintseva, N., and Abramov, A.: Thermal state of permafrost in Russia, Permafrost and
629   Periglacial Processes, 21, 136-155, 2010.
630 Salmon, V. G., Soucy, P., Mauritz, M., Celis, G., Natali, S. M., Mack, M. C., and Schuur, E. A.: Nitrogen
631   availability increases in a tundra ecosystem during five years of experimental permafrost thaw, Glob. Change
632   Biol., 22, 1927-1941, 2016.
633 Sanders, T., Fiencke, C., Fuchs, M., Haugk, C., Juhls, B., Mollenhauer, G., Ogneva, O., Overduin, P., Palmtag, J.,
634   and Povazhniy, V.: Seasonal nitrogen fluxes of the Lena River Delta, Ambio, 51, 423-438, 2022.
635 Schaller, J., Fauchere, S., Joss, H., Obst, M., Goeckede, M., Planer-Friedrich, B., Peiffer, S., Gilfedder, B., and
636   Elberling, B.: Silicon increases the phosphorus availability of Arctic soils, Scientific Reports, 9, 449, 2019.
637 Schaller, J. and Göckede, M., Pan-Arctic soil element availability estimations, doi:
638   https://doi.org/10.17617/3.8KGQUN, 2022.
639 Schaller, J., Puppe, D., Kaczorek, D., Ellerbrock, R., and Sommer, M.: Silicon Cycling in Soils Revisited, Plants,
640   10, 295, 2021.
641 Schirrmeister, L., Kunitsky, V., Grosse, G., Wetterich, S., Meyer, H., Schwamborn, G., Babiy, O., Derevyagin, A.,
642   and Siegert, C.: Sedimentary characteristics and origin of the Late Pleistocene Ice Complex on north-east
643   Siberian Arctic coastal lowlands and islands–A review, Quaternary international, 241, 3-25, 2011.
644 Schneider, M. P. W., Scheel, T., Mikutta, R., van Hees, P., Kaiser, K., and Kalbitz, K.: Sorptive stabilization of
645   organic matter by amorphous Al hydroxide, Geochim. Cosmochim. Acta, 74, 1606-1619, 2010.
646 Schuur, E., McGuire, A., Schädel, C., Grosse, G., Harden, J., Hayes, D., Hugelius, G., Koven, C., Kuhry, P.,
647   Lawrence, D., Natali, S., Olefeldt, D., Romanovsky, V., Schaefer, K., Turetsky, M., Treat, C., and Vonk, V.:
648   Climate change and the permafrost carbon feedback, Nature, 520, 171-179, 2015.
649 Schuur, E. A., Abbott, B., Bowden, W., Brovkin, V., Camill, P., Canadell, J., Chanton, J., Chapin, F., Christensen,
650   T., and Ciais, P.: Expert assessment of vulnerability of permafrost carbon to climate change, Climatic
651   Change, 119, 359-374, 2013.
652 Sher, A. V., Kuzmina, S. A., Kuznetsova, T. V., and Sulerzhitsky, L.: New insights into the Weichselian
653   environment and climate of the East Siberian Arctic, derived from fossil insects, plants, and mammals,
654   Quaternary science reviews, 24, 533-569, 2005.
655 Sims, J.: Comparison of Mehlich 1 and Mehlich 3 extractants for P, K, Ca, Mg, Mn, Cu and Zn in Atlantic coastal
656   plain soils, Commun. Soil Sci. Plant Anal., 20, 1707-1726, 1989.
657 Sowers, T. D., Wani, R. P., Coward, E. K., Fischel, M. H., Betts, A. R., Douglas, T. A., Duckworth, O. W., and
658   Sparks, D. L.: Spatially resolved organomineral interactions across a permafrost chronosequence, Environ.
659   Sci. Technol., 54, 2951-2960, 2020.
660 Strauss, J., Abbott, B. W., Hugelius, G., Schuur, E., Treat, C., Fuchs, M., Schädel, C., Ulrich, M., Turetsky, M., and
661   Keuschnig, M.: Permafrost, Recarbonizing global soils–A technical manual of recommended management
662   practices: Volume 2–Hot spots and bright spots of soil organic carbon, 2021a. 130, 2021a.

663 Strauss, J., Laboor, S., Schirrmeister, L., Fedorov, A. N., Fortier, D., Froese, D., Fuchs, M., Günther, F., Grigoriev,
664   M., and Harden, J.: Circum-Arctic Map of the Yedoma permafrost domain, Frontiers in Earth Science,
665   2021b. 1001, 2021b.
666 Strauss, J., Schirrmeister, L., Grosse, G., Fortier, D., Hugelius, G., Knoblauch, C., Romanovsky, V., Schädel, C.,
667   von Deimling, T. S., and Schuur, E. A.: Deep Yedoma permafrost: A synthesis of depositional characteristics
668   and carbon vulnerability, Earth-Sci. Rev., 172, 75-86, 2017.
669 Strauss, J., Schirrmeister, L., Grosse, G., Wetterich, S., Ulrich, M., Herzschuh, U., and Hubberten, H. W.: The deep
670   permafrost carbon pool of the Yedoma region in Siberia and Alaska, Geophys. Res. Lett., 40, 6165-6170,
671   2013.
672 Street, L. E., Mielke, N., and Woodin, S. J.: Phosphorus availability determines the response of tundra ecosystem
673   carbon stocks to nitrogen enrichment, Ecosystems, 21, 1155-1167, 2018.
674 Terhaar, J., Lauerwald, R., Regnier, P., Gruber, N., and Bopp, L.: Around one third of current Arctic Ocean primary
675   production sustained by rivers and coastal erosion, Nat. Commun., 12, 1-10, 2021.
676 Tremblay, J.-É., Anderson, L. G., Matrai, P., Coupel, P., Bélanger, S., Michel, C., and Reigstad, M.: Global and
677   regional drivers of nutrient supply, primary production and CO_2 drawdown in the changing Arctic Ocean,
678   Progress in Oceanography, 139, 171-196, 2015.
679 Walker, D., Bockheim, J., Chapin Iii, F., Eugster, W., Nelson, F., and Ping, C.: Calcium-rich tundra, wildlife, and
680   the "Mammoth Steppe", Quaternary Science Reviews, 20, 149-163, 2001.
681 Wiseman, C. and Püttmann, W.: Interactions between mineral phases in the preservation of soil organic matter,
682   Geoderma, 134, 109-118, 2006.
683 Yang, G., Peng, Y., Abbott, B. W., Biasi, C., Wei, B., Zhang, D., Wang, J., Yu, J., Li, F., and Wang, G.: Phosphorus
684   rather than nitrogen regulates ecosystem carbon dynamics after permafrost thaw, Glob. Change Biol., 27,
685   5818-5830, 2021.
686 Yurchenko, A. Y., Potapova, A., Bumagina, V., Vilesov, A., Chertina, K., Balushkina, N., Kalmykov, G., and
687   Khotylev, O.: Morphological and Lithogenetic Classification of the Carbonate Rocks of the Abalak–
688   Bazhenov Complex, Moscow University Geology Bulletin, 74, 372-379, 2019.
689 Zabel, M. and Schulz, H. D.: Marine geochemistry, Springer, 2006.

690